Research Square

Preprints are preliminary reports that have not undergone peer review.
They should not be considered conclusive, used to inform clinical practice,
or referenced by the media as validated information.

Hypervascular anterior mediastinal hyaline vascular-type Castleman disease with a feeding-vessel sign and intraoperative arterial bleeding: a case report

Zechen Cao[1]
The First Affiliated Hospital of Soochow University
Xiaoyu Qi[1]
The First Affiliated Hospital of Soochow University
Zhiwei Zhang[1]
zzwzhiwei@suda.edu.cn

The First Affiliated Hospital of Soochow University

Case Report

Keywords: Castleman disease, anterior mediastinum, hypervascular lesion, computed tomography, magnetic resonance imaging, video-assisted thoracoscopic surgery

Posted Date: November 19th, 2026

DOI: https://doi.org/10.21203/rs.3.rs-11106011/v1

License: This work is licensed under a Creative Commons Attribution 4.0 International License.
Read Full License

Additional Declarations: No competing interests reported.

Abstract

Background

Hyaline vascular-type Castleman disease is characterized by prominent vascular proliferation. When it occurs in the anterior mediastinum, its location and morphology may overlap with thymic tumors. Recognizing a hypervascular phenotype before minimally invasive resection is clinically important because unexpected arterial bleeding can complicate surgery.

Case presentation:

A 35-year-old man without constitutional or inflammatory symptoms was incidentally found to have a well-circumscribed left anterior mediastinal soft-tissue mass measuring approximately 49 × 25 mm. Mean attenuation increased from approximately 46 Hounsfield units (HU) on unenhanced computed tomography (CT) to 121 HU in the arterial phase (ΔHU ≈ 75 HU), with persistent delayed enhancement. Serial review of arterial-phase CT images suggested a feeding branch arising from the internal thoracic artery. On 3.0-T magnetic resonance imaging (MRI), the lesion was isointense on T1-weighted images and relatively hyperintense on T2-weighted images; diffusion-weighted imaging showed no definite high signal, whereas dynamic contrast-enhanced MRI demonstrated marked arterial enhancement with persistent delayed enhancement. Complete resection was achieved by single-port video-assisted thoracoscopic surgery. Bleeding from a mediastinal arterial branch occurred during dissection and was controlled intraoperatively. Histopathologic and immunohistochemical findings supported hyaline vascular-type Castleman disease. Follow-up noncontrast CT approximately 26 months after surgery showed no definite local recurrence.

Conclusions

In a well-circumscribed anterior mediastinal mass, disproportionate arterial enhancement, a traceable feeding vessel, and persistent enhancement should raise suspicion for a hypervascular lesion and prompt deliberate planning for vascular control. These findings are not specific for Castleman disease, and definitive diagnosis remains histopathologic, but preoperative recognition of hypervascularity may reduce avoidable surgical risk.

Background

Castleman disease (CD) is a rare lymphoproliferative disorder characterized by distinctive histopathologic changes in lymph nodes. Clinically, CD is generally classified as unicentric Castleman disease (UCD) or multicentric Castleman disease. UCD is typically confined to a single lymph node or nodal region, often lacks prominent systemic inflammatory manifestations, and frequently involves the

mediastinum among intrathoracic sites. For resectable UCD, complete surgical excision is the mainstay of treatment and is generally associated with a favorable prognosis [1–3].

The hyaline vascular type, also termed the hypervascular pattern, is the most common histopathologic pattern of UCD, and its imaging appearance reflects prominent vascular proliferation. Thoracic lesions often present as well-circumscribed soft-tissue masses with marked enhancement and may be accompanied by enlarged feeding or draining vessels [4–7]. In the anterior mediastinum, however, these lesions overlap anatomically with thymic tumors, and underestimating vascularity can increase the risk of bleeding during thoracoscopic dissection.

We report a localized anterior mediastinal hyaline vascular-type Castleman disease in which quantitative CT enhancement, dynamic contrast-enhanced MRI, a feeding-vessel sign, intraoperative arterial bleeding, and pathology were directly correlated. The educational focus is the preoperative recognition of a hypervascular phenotype and its implications for operative planning rather than diagnosis from any single imaging feature.

Case presentation

A 35-year-old man was admitted on May 22, 2023 after an anterior mediastinal mass had been incidentally detected during a routine health examination approximately 5 days earlier. He reported no fever, chills, night sweats, weight loss, cough, sputum production, chest tightness, or dyspnea. His medical and family histories were unremarkable. No superficial lymphadenopathy was palpable, and cardiopulmonary and abdominal examinations were unremarkable. The preoperative complete blood count showed no obvious abnormalities, and postoperative blood counts also remained unremarkable.

Noncontrast chest CT performed on May 17, 2023 showed a left-sided anterior mediastinal soft-tissue mass measuring approximately 49 × 24 mm with relatively well-defined margins. Contrast-enhanced CT on May 23, 2023 demonstrated a lesion measuring approximately 49 × 25 mm with marked enhancement. Quantitative analysis of the unenhanced and corresponding enhanced images was performed using DICOM Viewer software. A 1-cm² region of interest (ROI) was placed in the central portion of the lesion, avoiding visible vessels and peripheral partial-volume effects whenever possible. Mean attenuation was approximately 46 HU on unenhanced CT and 121 HU in the arterial phase, corresponding to a net increase of approximately 75 HU. The lesion remained strongly enhanced on delayed-phase images. Serial review of arterial-phase axial images suggested a feeding branch arising from the internal thoracic artery, and enlarged tortuous vessels were visible along the lesion periphery. No definite destruction of adjacent structures was identified (Fig. 1). Given the anatomic location, the preoperative imaging diagnosis favored a thymic-origin tumor.

Chest MRI was performed at 3.0 T on May 24, 2023. The lesion measured approximately 46 × 26 mm and was well circumscribed. It was isointense on T1-weighted images and relatively hyperintense on T2-weighted images. Diffusion-weighted imaging was acquired at b values of 50 and 800 s/mm²; the lesion showed no definite high signal, while the apparent diffusion coefficient map showed relatively high

signal. Dynamic contrast-enhanced MRI demonstrated marked arterial-phase enhancement with persistent delayed enhancement. Coronal images confirmed the left anterior mediastinal location and relatively clear interfaces with adjacent structures (Fig. 2). MRI further supported the hypervascular nature of the lesion but did not establish a specific histopathologic diagnosis.

On May 25, 2023, the patient underwent single-port video-assisted thoracoscopic resection of the left anterior mediastinal lesion under general anesthesia. Intraoperatively, the mass was located in the left anterior mediastinum. Bleeding from a mediastinal arterial branch occurred during dissection; hemostasis was achieved promptly, and the lesion was completely resected. Frozen-section examination showed lymph node tissue with lymphoid hyperplasia. The final diagnosis was established on paraffin-embedded sections and immunohistochemical staining.

The gross specimen measured approximately 7 × 6 × 3 cm. On sectioning, an encapsulated mass measuring approximately 5 × 4 × 2 cm was identified. Immunohistochemistry showed nodular positivity for CD20 and CD79a and partial positivity for CD2 and CD3. CD10 and BCL6 were expressed predominantly in germinal centers, while CD21 and CD23 highlighted follicular dendritic cell networks. The Ki-67 proliferation index was approximately 5%, and Cyclin D1, TdT, and SOX11 were negative. Together with the histologic morphology, these findings supported hyaline vascular-type Castleman disease (Fig. 3). Because standardized whole-body staging had not been performed, the case is described as localized anterior mediastinal hyaline vascular-type Castleman disease rather than formally staged UCD.

The postoperative course was uneventful, and the patient was discharged on May 28, 2023. Follow-up noncontrast chest CT on July 9, 2025, approximately 26 months after surgery, showed no definite abnormal soft-tissue mass or evidence of local recurrence at the original anterior mediastinal site (Fig. 4).

Discussion and Conclusions

Among intrathoracic presentations of Castleman disease, localized/UCD lesions may be discovered incidentally in asymptomatic patients [1–3]. For the hyaline vascular pattern, the most informative imaging feature is often not the anatomic location itself but the degree and pattern of vascularity. Prior studies have described homogeneous or marked enhancement and enlarged feeding or draining vessels in thoracic lesions [5–7]. In the anterior mediastinum, these findings are clinically useful because location alone can readily suggest a thymic-origin tumor.

Quantitative enhancement provided an additional clue in the present case. Using a 1-cm² ROI, mean attenuation increased from approximately 46 HU on unenhanced CT to 121 HU in the arterial phase, a net increase of approximately 75 HU, and enhancement persisted on delayed images. More importantly, serial review of arterial-phase axial CT images suggested a feeding branch connected to the internal thoracic artery. Together, marked arterial enhancement, a visible feeding-vessel sign, and persistent delayed enhancement constituted a hypervascular imaging phenotype. The proposed origin of the

feeding vessel was inferred from serial CT images and was not confirmed by CT angiography, digital subtraction angiography, or selective catheter angiography; therefore, the vascular anatomy should be described as suggestive rather than definitive.

This imaging hypervascularity has a pathologic basis. Hyaline vascular-type Castleman disease typically shows interfollicular capillary proliferation, hyalinized small vessels, and abnormal follicular architecture. Park et al. demonstrated a correlation between the degree of CT enhancement and histologic microvessel density, supporting the concept that enhancement reflects lesion vascularity [8]. Classic regressed germinal centers, concentrically arranged mantle zones, and hyalinized vessels penetrating follicles are useful histologic features [9]. In the present case, conventional histology together with nodular B-cell distribution on CD20/CD79a, follicular dendritic cell networks highlighted by CD21/CD23, and a low Ki-67 proliferation index supported the diagnosis.

MRI mainly provided complementary information regarding tissue signal and dynamic enhancement. Previous reports describe Castleman disease as commonly iso- or hypointense on T1-weighted images, iso- or hyperintense on T2-weighted images, and markedly enhancing; vascular flow voids may also be present [5, 10, 11]. MR angiography has demonstrated feeding vessels in individual mediastinal cases [12]. In our patient, 3.0-T diffusion-weighted imaging showed no definite high signal, whereas dynamic contrast-enhanced MRI confirmed marked arterial enhancement with persistent delayed enhancement. Its main contribution was therefore confirmation of the hypervascular pattern and delineation of the lesion's anatomic boundaries.

The principal clinical implication is operative risk management. The rich blood supply of Castleman disease can produce substantial intraoperative bleeding, and preoperative embolization has been used in selected hypervascular mediastinal lesions [2, 13]. Thoracoscopic resection is feasible in appropriately selected intrathoracic UCD [14], but recent case literature illustrates why vascular planning matters: a 2025 posterior mediastinal case required conversion from VATS to thoracotomy because of significant bleeding and adhesions [16], whereas a 2026 intrathoracic case used preoperative embolization before robotic resection and reported blood loss of less than 100 mL [17]. In our patient, complete resection was achieved through a single-port thoracoscopic approach, but arterial-branch bleeding occurred during dissection, concordant with the preoperative hypervascular imaging features. For similar lesions, preoperative assessment should systematically address vascularity, the relationship to major vessels, and options for proximal vascular control. In larger, anatomically complex, or clearly feeder-dominant lesions, angiographic evaluation and embolization may be considered on an individualized basis rather than as a routine step for all patients.

Anterior mediastinal Castleman disease can overlap with low-risk thymoma and other lesions in margins, morphology, and enhancement. Accordingly, imaging should not be used to diagnose Castleman disease from a single attenuation threshold. Instead, disproportionate arterial enhancement, a traceable feeding vessel, persistent enhancement, and an absence of invasive features should prompt consideration of

Castleman disease or another hypervascular lesion and should alert the surgical team to potential bleeding risk [4, 9, 15]. Definitive characterization still requires histopathologic examination.

In conclusion, localized anterior mediastinal hyaline vascular-type Castleman disease may present as a well-circumscribed but markedly hypervascular soft-tissue mass. In this case, quantitative CT enhancement, a suspected feeding branch, persistent enhancement on CT and MRI, intraoperative arterial bleeding, and the final pathology formed a coherent radiologic-surgical-pathologic correlation. For comparable anterior mediastinal lesions, recognizing the hypervascular phenotype before surgery may improve preparation for vascular control and minimally invasive resection, even when imaging cannot establish the final diagnosis.

Abbreviations

ADC
apparent diffusion coefficient
CD
Castleman disease
CT
computed tomography
DWI
diffusion-weighted imaging
HU
Hounsfield units
MRI
magnetic resonance imaging
ROI
region of interest
UCD
unicentric Castleman disease
VATS
video-assisted thoracoscopic surgery.

Declarations

Consent for publication

Written informed consent was obtained from the patient for publication of this case report and the accompanying images.

Competing interests

The authors declare that they have no competing interests.

Funding

This work was supported by the Gusu Health Talent Program of Suzhou [GSWS2023078].

Author Contribution

Z.C and X.Q contributed equally to data curation, imaging analysis, literature review, and drafting of the manuscript. Z.Z conceived and supervised the report and critically revised the manuscript for important intellectual content. All authors read and approved the final manuscript.

Availability of data and materials

All data generated or analyzed during this study are included in this article. Additional patient-level data are not publicly available to protect privacy but may be available from the corresponding author on reasonable request and subject to applicable ethical and institutional requirements.

References

1. Dispenzieri A, Fajgenbaum DC. Overview of Castleman disease. Blood. 2020;135(16):1353–64. 10.1182/blood.2019000931.
2. van Rhee F, Oksenhendler E, Srkalovic G, et al. International evidence-based consensus diagnostic and treatment guidelines for unicentric Castleman disease. Blood Adv. 2020;4(23):6039–50. 10.1182/bloodadvances.2020003334.
3. Luo JM, Li S, Huang H, et al. Clinical spectrum of intrathoracic Castleman disease: a retrospective analysis of 48 cases in a single Chinese hospital. BMC Pulm Med. 2015;15:34. 10.1186/s12890-015-0019-x.
4. Pitot MA, Tahboub Amawi AD, Alexander LF, et al. Imaging Castleman Disease Radiographics. 2023;43(8):e220210. 10.1148/rg.220210.
5. Zhao S, Wan Y, Huang Z, Song B, Yu J. Imaging and clinical features of Castleman Disease. Cancer Imaging. 2019;19(1):53. 10.1186/s40644-019-0238-0.
6. Kwon S, Lee KS, Ahn S, Song I, Kim TS. Thoracic Castleman disease: computed tomography and clinical findings. J Comput Assist Tomogr. 2013;37(1):1–8. 10.1097/RCT.0b013e318270658b.
7. Hoshiai S, Watadani T, Kagaya S, et al. Imaging of unicentric hyaline-vascular variant of Castleman disease: emphasis on perilesional fat stranding and fatty proliferation. Glob Health Med. 2024;6(6):375–82. 10.35772/ghm.2024.01058.

8. Park SH, Cho A, Ryu HJ, Kim H. Profile of vascular markers and CT enhancement of hyaline vascular type Castleman's disease. Microvasc Res. 2022;142:104357. 10.1016/j.mvr.2022.104357.
9. Kligerman SJ, Auerbach A, Franks TJ, Galvin JR. Castleman Disease of the Thorax: Clinical, Radiologic, and Pathologic Correlation: From the Radiologic Pathology Archives. Radiographics. 2016;36(5):1309–32. 10.1148/rg.2016160076.
10. Hill AJ, Tirumani SH, Rosenthal MH, et al. Multimodality imaging and clinical features in Castleman disease: single institute experience in 30 patients. Br J Radiol. 2015;88(1049):20140670. 10.1259/bjr.20140670.
11. Moon WK, Im JG, Han MC. Castleman's disease of the mediastinum: MR imaging features. Clin Radiol. 1994;49(7):466–8. 10.1016/S0009-9260(05)81742-8.
12. Ecklund K, Hartnell GG. Mediastinal Castleman disease: MR and MRA features. J Thorac Imaging. 1994;9(3):156–9. 10.1097/00005382-199422000-00007.
13. Amano Y, Takai D, Ohishi N, et al. Successful treatment of mediastinal unicentric Castleman's disease using video-assisted thoracoscopic surgery with preoperative embolization. Case Rep Med. 2013;2013:354507. 10.1155/2013/354507.
14. Wang YQ, Li SQ, Guo F. Video-assisted thoracoscopic surgery is a safe and effective method to treat intrathoracic unicentric Castleman's disease. BMC Surg. 2020;20(1):127. 10.1186/s12893-020-00789-6.
15. Din F, Mellor F, Millard T, et al. Radiology of Castleman disease: the pivotal role of imaging in diagnosis, staging, and response assessment of this rare entity. Clin Radiol. 2022;77(6):399–408. 10.1016/j.crad.2022.01.045.
16. Belayachi B, Fenane H, Msougar Y. Surgical approach to posterior mediastinal Castleman’s disease: a case report. Pan Afr Med J. 2025;50:54. 10.11604/pamj.2025.50.54.45984.
17. Leite FF, Santos RS, Falsarella PM, et al. Preoperative embolization and lung-sparing robotic surgery in intrathoracic Castleman’s disease: case report. J Vasc Bras. 2026;25:e20250167. 10.1590/1677-5449.202501672.

Figures

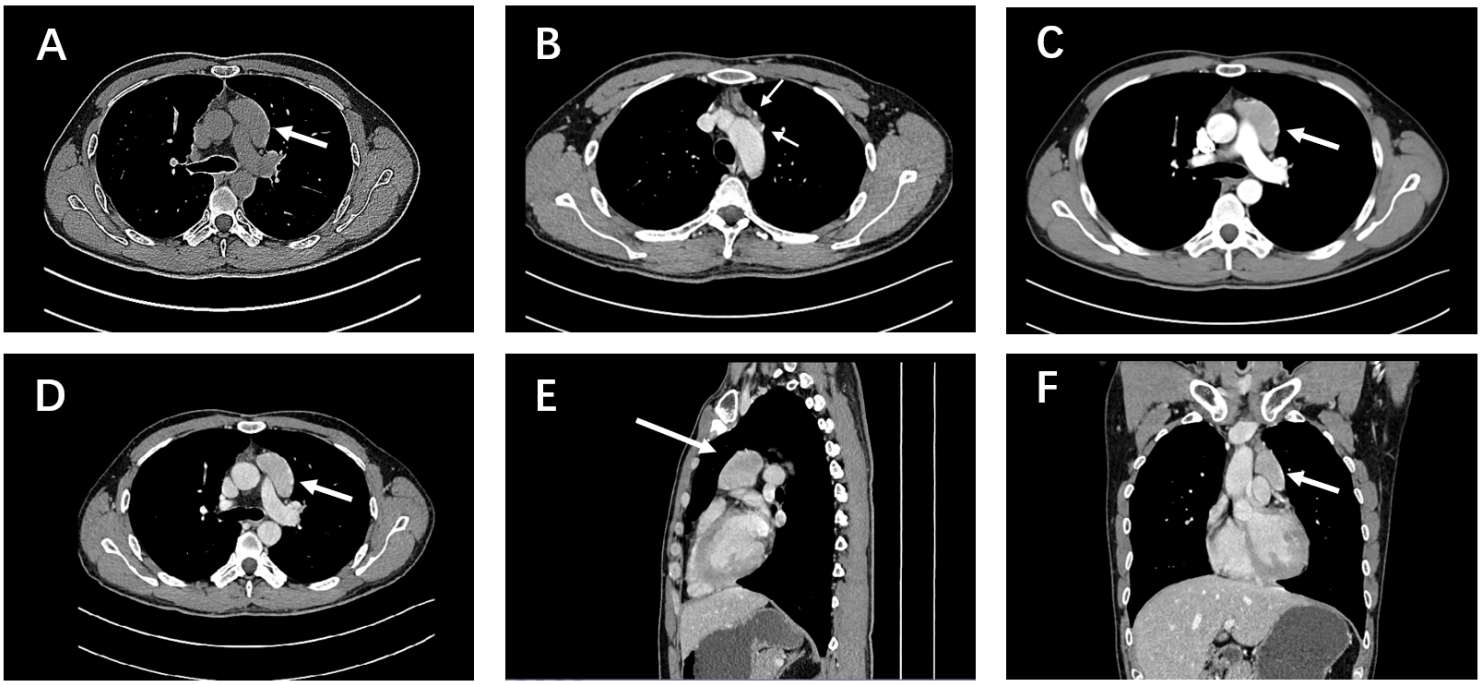


Figure 1

Preoperative CT findings and quantitative enhancement. (A) Axial noncontrast CT obtained on May 17, 2023 shows a relatively well-circumscribed soft-tissue mass in the left anterior mediastinum, with a mean attenuation of approximately 46 HU. (B) Axial arterial-phase contrast-enhanced CT obtained on May 23, 2023; serial review suggests a feeding branch arising from the internal thoracic artery. (C) Arterial-phase CT demonstrates marked tumor enhancement, with a mean ROI attenuation of approximately 121 HU, representing a net increase of approximately 75 HU from the unenhanced scan. (D) Delayed-phase CT shows persistent marked enhancement. (E) Sagittal contrast-enhanced CT reconstruction demonstrates the anteroposterior dimension of the lesion and its relationship to adjacent structures. (F) Coronal contrast-enhanced CT reconstruction shows the long axis, lesion margins, and anterior mediastinal location.

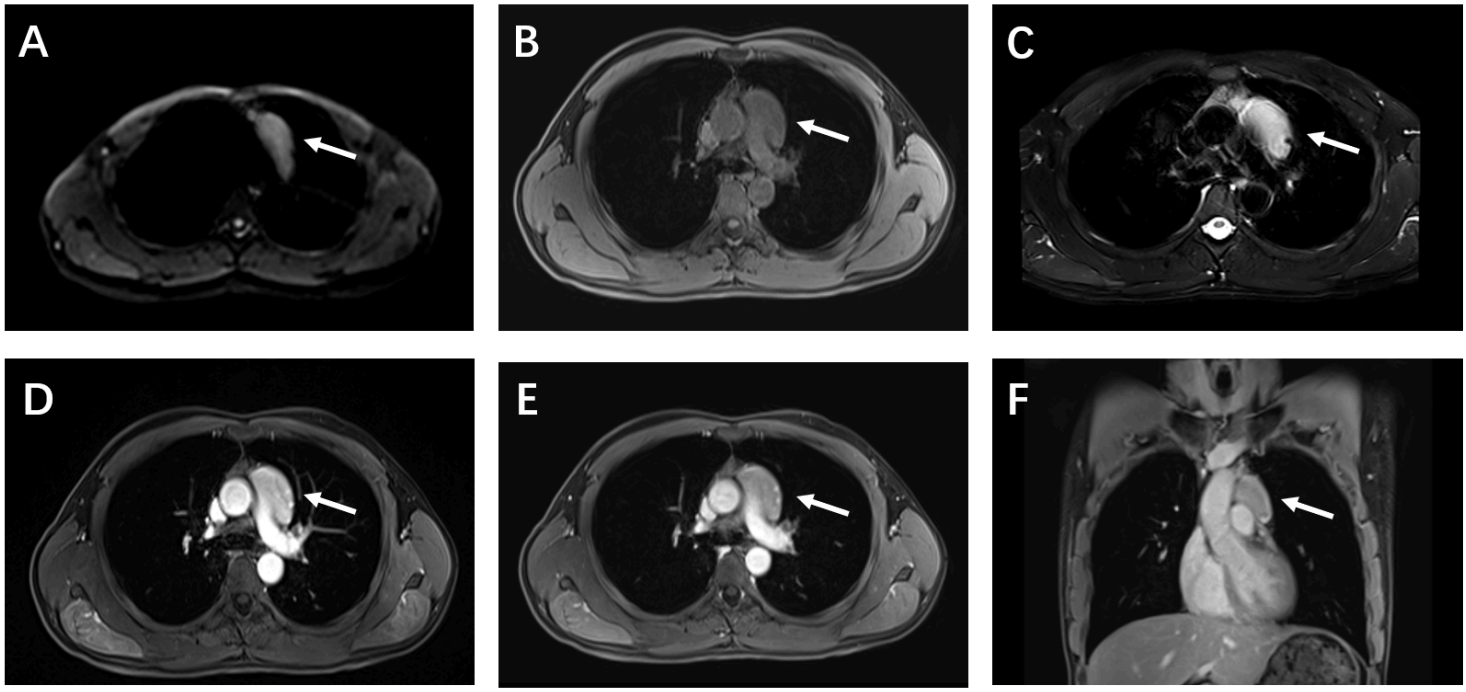


Figure 2

Preoperative MRI findings. Imaging was performed on a 3.0-T system. (A) No definite diffusion hyperintensity is seen; DWI was acquired at b values of 50 and 800 s/mm². (B) Axial unenhanced T1-weighted image shows the lesion to be isointense. (C) Axial unenhanced T2-weighted image shows relatively high signal intensity and well-defined margins. (D) Axial arterial-phase dynamic contrast-enhanced MRI demonstrates marked enhancement. (E) Delayed-phase axial image shows persistent enhancement. (F) Contrast-enhanced coronal image demonstrates the lesion in the left anterior mediastinum and its anatomic relationship to surrounding structures.

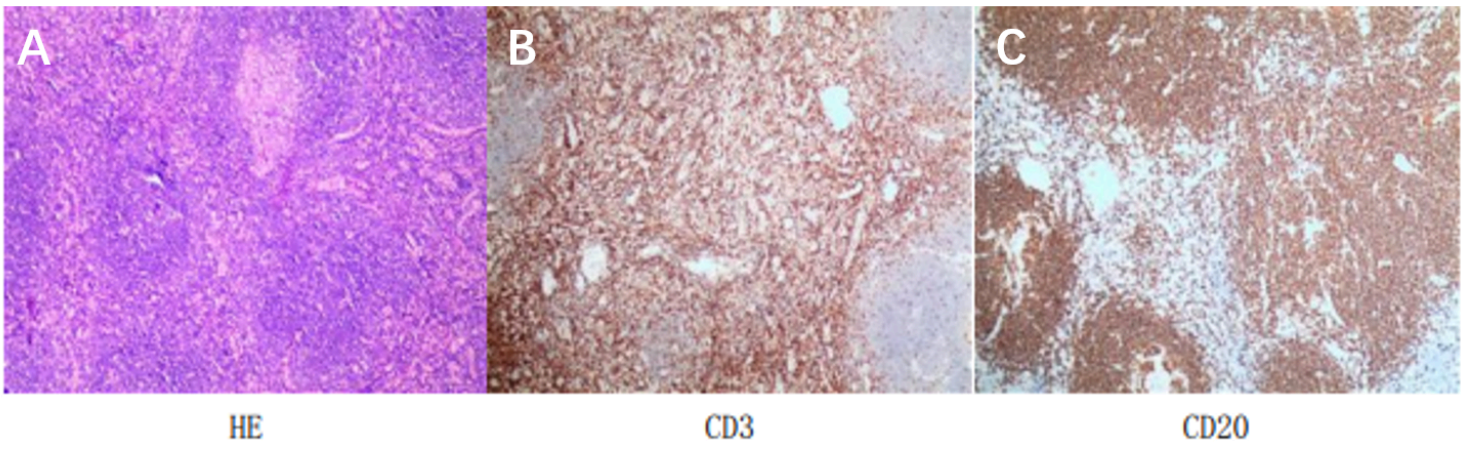


Figure 3

Histopathologic and immunohistochemical findings. (A) Low-power hematoxylin and eosin (H&E) image shows the overall lymphoid architecture of the lesion. Because a high-power H&E image was not available, this panel is included only to demonstrate the general tissue architecture. (B) CD3

immunohistochemistry highlights T-cell areas. (C) CD20 immunohistochemistry shows a nodular distribution of B cells. Additional reported immunohistochemical findings included nodular CD79a positivity, follicular dendritic cell networks highlighted by CD21/CD23, predominant germinal-center expression of CD10/BCL6, negativity for Cyclin D1, TdT, and SOX11, and a Ki-67 proliferation index of approximately 5%. Taken together with the morphology and immunophenotype, the findings supported hyaline vascular-type Castleman disease.

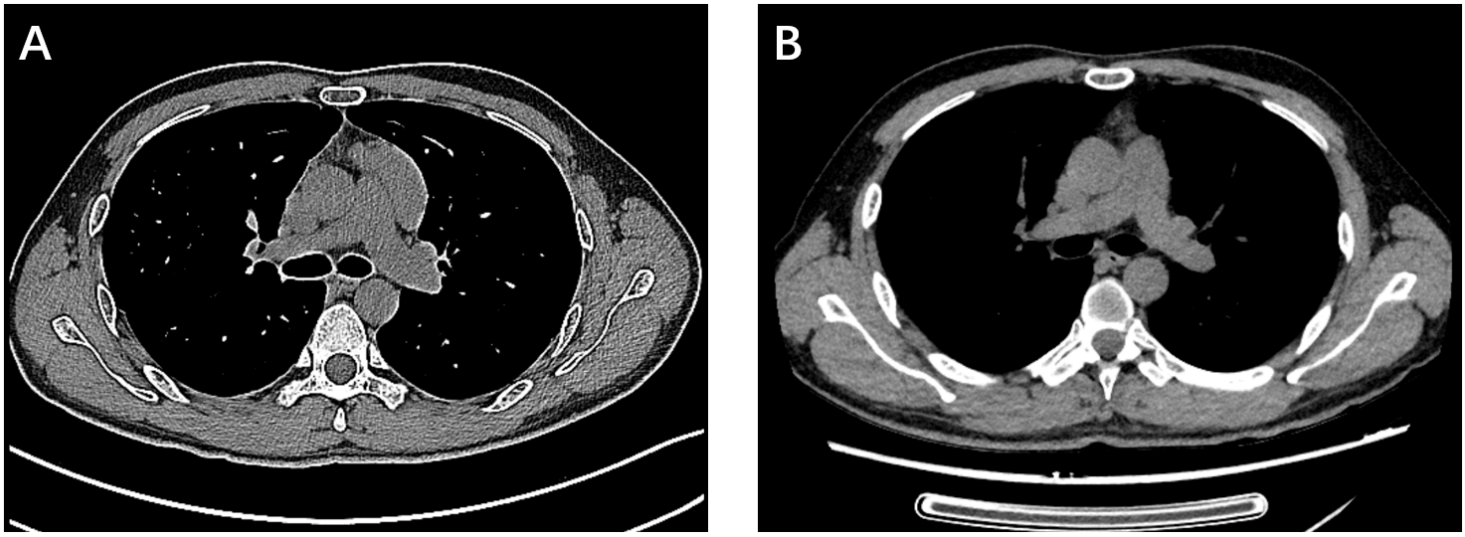


Figure 4

CT before and after surgery. (A) Preoperative anterior mediastinal mass. (B) At approximately 26 months, noncontrast CT shows no definite local recurrence.